

Research Article

Local heterogeneity analysis of crystallographic and cryo-EM maps using shell-approximation

Vladimir Y. Lunin^{a,*}, Natalia L. Lunina^a, Alexandre G. Urzhumtsev^{b,c,**}^a Institute of Mathematical Problems of Biology RAS, Keldysh Institute of Applied Mathematics of Russian Academy of Sciences, 1, Professor Vitkevich St., Pushchino, 142290, Russia^b Centre for Integrative Biology (CBI), Department of Integrated Structural Biology, IGBMC (Institute of Genetics and of Molecular and Cellular Biology), 1 rue Laurent Fries, Illkirch, France^c Université de Lorraine, Faculté des Sciences et Technologies, BP 239, 54506, Vandoeuvre-les-Nancy, France

ARTICLE INFO

Handling Editor: Prof N Ban

Keywords:

Real-space refinement
Inhomogeneous resolution
Atomic images
Shell decomposition

ABSTRACT

In X-ray crystallography and cryo-EM, experimental maps can be heterogeneous, showing different level of details in different regions. In this work we interpret heterogeneity in terms of two parameters, assigned individually for each atom, combining the conventional atomic displacement parameter with the resolution of the atomic image in the map. We propose a local real-space procedure to estimate the values of these heterogeneity parameters, assuming that a fragment of the density map and atomic positions are given. The procedure is based on an analytic representation of the atomic image, as a function of the inhomogeneity parameters and atomic coordinates. In this article, we report the results of the tests both with maps simulated and those derived from experimental data. For simulated maps containing regions with different resolutions, the method determines the local map resolution around the atomic centers and the values of the displacement parameter with reasonable accuracy. For experimental maps, obtained as a Fourier synthesis of a given global resolution, estimated values of the local resolution are close to the global one, and the values of the estimated displacement parameters are close to the respective values of the closest atoms in the refined model. Shown successful applications of the proposed method to experimental crystallographic and cryo-EM maps can be seen as a practical proof of method.

1. Introduction

Electron density distribution corresponding to a given atomic model is a key element in real-space fitting and refinement of macromolecular structures in X-ray crystallography (Rupp, 2009; Urzhumtsev and Lunin, 2019). For an appropriate quantitative comparison of a theoretical map (calculated from an available atomic model) with an experimental one, the theoretical map should mimic the distortions of the experimental one. Considering that experimental errors and data imperfections, including their incompleteness, already have been treated in the best possible way, the two main sources of distortions of the experimental map at the late stages of structure determination are dynamic and static variation in atomic positions and a limited resolution with which the atoms are represented by the map.

Both the scale of the positional variations (positional uncertainty) and the resolution of atomic images may change within the sample. Inside the macromolecular region, one may attribute them to each atom individually. In a recent series of papers (Urzhumtsev and Lunin, 2022a, 2022b; Urzhumtsev et al., 2022; Urzhumtseva et al., 2023), an efficient procedure has been proposed to calculate images of individual atoms adapted to distortions of the experimental map, provided the coordinates, atomic displacement parameter (ADP), and the atomic image resolution (AIR). In this article, we discuss an approach to solve the inverse problem, that, given a map and atomic coordinates, to find the local ADP and AIR values for each atom of the structure. These values reflect the level of heterogeneity of the experimental map and can be used as initial values for further crystallographic refinement of these parameters (Urzhumtsev and Lunin, 2022b). The proposed approach is

Abbreviations: ADP, Atomic Displacement Parameter; AIR, Atomic Image Resolution.

* Corresponding author. Institute of Mathematical Problems of Biology RAS, 1, Professor Vitkevich St., Pushchino, 142290, Russia.

** Corresponding author. Centre for Integrative Biology (CBI), Department of Integrated Structural Biology, IGBMC (Institute of Genetics and of Molecular and Cellular Biology), 1 rue Laurent Fries, Illkirch, France.

E-mail addresses: lunin@impb.ru (V.Y. Lunin), lunina@impb.ru (N.L. Lunina), sacha@igbmc.fr (A.G. Urzhumtsev).

<https://doi.org/10.1016/j.crstbi.2023.100102>

Received 28 December 2022; Received in revised form 1 June 2023; Accepted 5 June 2023

Available online 15 June 2023

2665-928X/© 2023 The Authors. Published by Elsevier B.V. This is an open access article under the CC BY-NC-ND license (<http://creativecommons.org/licenses/by-nc-nd/4.0/>).

currently aimed to the range from medium to high resolution (1.5–3.5 Å), does not consider anisotropy of atomic images, the presence of deformation density (Bragg, 1920) and ignores errors in atomic positions (e.g., Cruickshank, 1999; Gurusaran et al., 2014; and references therein). The capability of the method to reproduce these distortion parameters and experimental maps allows addressing the following step, namely a common refinement of atomic positions and these parameters.

The previous considerations are also applicable to experimental maps other than electron density distribution, for example, to maps of the electrostatic scattering potential studied by cryo electron microscopy (cryo-EM), nuclear density in studies of neutron diffraction, and other maps which can be represented by a sum of contributions of individual atoms. Below, to be short, we will call all such maps as ‘density distribution’ maps.

In such methods, the samples contain a huge number of molecules, in which the same parts may occur in different conformations (static disorder). Furthermore, any atom may vary its position due to thermal motion (dynamic disorder). Dynamic and static disorder blur the density peaks in the maps which show an average molecular image and are usually modeled by convolution of the theoretical atomic density with a Gaussian function, individual for each atom. This function defines the probability of the displacement of the atom from its mean position. Below we consider the isotropic case only, specifying the width of the Gaussian distribution by a single parameter B (atomic displacement parameter). This parameter is related to the mean square displacement $\langle |u|^2 \rangle$ of the atom in three-dimensional space by $B = (8\pi^2 \langle |u|^2 \rangle) / 3$. Convolution in real space with such function is equivalent to multiplication of the atomic scattering factor by $\exp[-B(\sin \theta / \lambda)^2]$ where 2θ is the angle between the incident and reflected X-ray beams and λ is the wavelength. Previously, some methods to calculate atomic images in the maps of a given resolution knowing the ADP values, and eventually to refine these values, have been suggested by Diamond (1971), Lunin and Urzhumtsev (1984), Chapman (1995), Mooij et al. (2006), Chapman et al. (2013), DiMaio et al. (2015), Pintilie et al. (2020).

The term ‘resolution’ has different meaning in different fields of science and different experimental techniques. In macromolecular crystallography, the most commonly, the resolution of density map is defined in terms of the Fourier transform $F(\mathbf{s})$ of the density distribution (e.g., Rupp, 2009). When working with a crystal, real or virtual, the Fourier transform is reduced to a discrete set of Fourier coefficients (structure factors), corresponding to the reciprocal space lattice. Initially, a resolution value d is attributed to each individual reflection, to the corresponding scattering vector \mathbf{s} , and to the structure factor $F(\mathbf{s})$. Numerically, it is defined as $d = |\mathbf{s}|^{-1} = \lambda / (2 \sin \theta)$. Then, this term is extended to the sets of reciprocal space vectors \mathbf{s} that include all (or almost all) vectors with $|\mathbf{s}| \leq d_{\min}^{-1}$. The value d_{\min} is called the resolution of the respective data set which we note as $S(d_{\min})$. Similarly, this term d_{\min} is applied to define the formal resolution of the map calculated as a Fourier synthesis

$$\rho^d(\mathbf{r}; d_{\min}) = \frac{1}{V_{\text{cell}}} \sum_{\mathbf{s} \in S(d_{\min})} \mathbf{F}(\mathbf{s}) \exp[-i2\pi\mathbf{s} \cdot \mathbf{r}] \quad (1)$$

over such set $S(d_{\min})$ of reciprocal space lattice vectors. Here V_{cell} is the unit cell volume and $\mathbf{s} \cdot \mathbf{r}$ is the dot (scalar) product of two vectors. The resolution value d corresponding to a particular structure factor $F(\mathbf{s})$ is numerically equal to the period of the associated Fourier harmonic $\psi_{\mathbf{s}}(\mathbf{r}) = \exp[-i2\pi\mathbf{s} \cdot \mathbf{r}]$ in the direction \mathbf{s} , so that the value d_{\min} is sometimes referred to as the full-period Fourier resolution of the synthesis (1). A positional uncertainty, described by the convolution of $\rho^d(\mathbf{r}; d_{\min})$ with a Gaussian, is equivalent to a Gaussian weighting of structure factors reducing their magnitudes. To describe individual atomic uncertainties, such weight should be applied to individual atomic contributions to $F(\mathbf{s})$.

The truncation of the resolution limit causes blurring the peaks and appearance of Fourier series terminations ripples (James, 1948), a series

of spherical shells of alternative sign map values, surrounding the atomic center. While not exceeding in amplitude, 10% of the height of the central peak, these ripples may produce visible distortions in maps in a large range of resolution, e.g., hiding density peaks for water molecules at resolution around 3 Å (Minichino et al., 2003) or producing false features mimicking deformation density in ultra-high-resolution studies (Afonine et al., 2004, Fig. 4). The effect of the truncation of resolution in Fourier synthesis (1) may be described as the convolution of the theoretical distribution with the three-dimensional interference function (Urzhumtsev and Lunin, 2022a).

In crystallography, high-resolution data are cut-out directly during experiment, data processing is done in reciprocal space and the effects of data errors, manipulations and truncation are propagated evenly over the whole structure. In cryo-EM, a number of higher-resolution Fourier harmonics are also missed due to experimental features. Even when some of them are formally present, they are negligibly small in practice (Afonine et al., 2018). Differently from crystallography, cryo-EM image-processing procedures are done essentially in real space (as a recent example, combine focused maps by Liebschner et al., 2019). Respectively, different parts of cryo-EM maps may be described by different sets of Fourier harmonics.

The resolution in cryo-EM is usually estimated by comparing, in resolution shells, structure factors calculated from two maps (half-maps) reconstructed independently from two different subsets of experimental data (van Heel et al., 1982; Saxton and Baumeister, 1982; Rosenthal and Henderson, 2003; van Heel and Schatz, 2017). The key difference from the ‘crystallographic’ definition is that the latter tells how many Fourier harmonics are present in the map, while the cryo-EM definition, based on the Fourier Shell Correlation function (FSC), tells how many of them are reliable.

There exist other approaches to define the resolution. Addressing the question of the data strength, the resolution may be declared as the limit beyond which excluding structure factors does not affect atomic model refinement (Karplus and Diederichs, 2012) or the maps themselves (Afonine et al., 2018). Alternatively, one can define the resolution value addressing directly to the map’s features. For example, one can analyze the Model Trapping Function (Pintilie and Chiu, 2012; Lunin et al., 2019), which shows the number of atoms inside the region of the highest density values varying the cut-off value. Also, one can define the resolution from the ‘optical features’ of the map (Vaguine et al., 1999; Penczek, 2010; Urzhumtseva et al., 2013). Some discussions concerning comparison of different resolution definitions and respective terms can be found in Liao and Frank (2010), Penczek (2010), Evans and Murshudov (2013), Afonine et al. (2018). In what follows, we consider the term ‘resolution’ in the crystallographic meaning associated with (1).

The formal resolution value of the Fourier synthesis (1) characterizes the macromolecular image in the map as a whole while details of different parts of this image may be different. For example, Fig. 1 shows an image of four tyrosine residues inside the same virtual crystal cell. This image was calculated as a single Fourier synthesis of a formal resolution equal to 2 Å. The fragment A reproduces the features of a typical 2 Å resolution map, while the fragment C looks like a 5 Å-resolution one. The fragment B demonstrates the effect of increasing the ADP values of all atoms to 100 Å². Fragment D reveals the features of images of a resolution higher than 2 Å, while actually being a sharpened (Terwilliger et al., 2018) 2 Å-resolution image. Thus, to evaluate properly the quality of a map, a single global characteristic is insufficient (Cardone et al., 2013) and some parameters characterizing local features are required (Chapman et al., 2013; Kucukelbir et al., 2014; Vilas et al., 2018; Ramírez-Aportela et al., 2019).

In our approach (Urzhumtsev and Lunin, 2022a), to model the distortions in the experimental map, we attribute two individual heterogeneity parameters to every atom. The first one is the standard isotropic atomic displacement parameter B_{atom} . The second parameter is atomic image resolution D_{atom} which reflects the local resolution of the experimental map around the center of the atom. While the first parameter

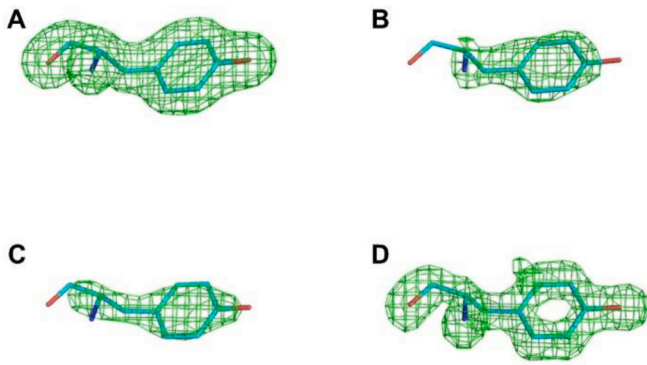


Fig. 1. Fourier synthesis calculated as (1) with the resolution $d_{min} = 2 \text{ \AA}$ reproduces the features of the nominal resolution map (A) and those of lower (B, C) and higher (D) resolution. Structure factors used to calculate this synthesis were the sums of structure factors from four sets, corresponding to the fragments: A) 2 \AA -resolution set of structure factors for atoms with $B = 20 \text{ \AA}^2$; B) 2 \AA -resolution set of structure factors for atoms with B increased to 100 \AA^2 ; C) the same as in A) where all structure factors in the range 2–5 \AA -resolution were artificially assigned to be equal to zero; D) a set of structure factors calculated with point-atom scattering factors in the resolution range from 2 \AA to 5 \AA and zero structure factors outside this range.

describes a Gaussian-shape attenuation of the magnitudes of Fourier coefficient with resolution, the second parameter stands for other kinds of their absence or reduction, in particular a sharp cut-off in crystallography. We call these parameters the ‘point’ atomic heterogeneity parameters since they are attributes of an isolated atom, without considering its environment. The proposed analytical formulas to calculate model density values and their derivatives with respect to the resolution D_{atom} allow us to include the parameters $\{D_{atom,n}, n = 1, 2, \dots, N_{atoms}\}$ in the gradient-driven real-space crystallographic refinement (Urzhumtsev and Lunin, 2022b) similarly to ADP refinement.

We may also estimate the local heterogeneity of a given map calculating heterogeneity parameters in different small regions, referred to as vicinities. To do so, for a given reference point \mathbf{r}_{ref} in space we define the local heterogeneity parameters values B_{vic}, D_{vic} obtained under the assumption that all atoms neighboring to \mathbf{r}_{ref} have the same B_{atom} and D_{atom} values equal to B_{vic}, D_{vic} . The values B_{vic}, D_{vic} are determined by minimizing the discrepancy between the calculated and observed maps in a vicinity of the reference point. While any space point can be chosen as a reference one, below we consider only the centers of atoms as the reference points. This allows us to consider the local values $B_{vic,n}, D_{vic,n}$ found in a vicinity of the atom n as estimates of the point heterogeneity parameters $B_{atom,n}, D_{atom,n}$ of this atom.

A particular difficulty to estimate the local ADP value B_{vic} and the local resolution D_{vic} in a vicinity of a given atom is that both factors blur the density peaks somehow similarly. Thus, a decrease in the height and an increase in the width of the central peak of the atomic image can be described by increasing any of B_{vic} and D_{vic} values (see fragments B and C in Fig. 1). The major difference between the two effects is that limiting the resolution results in Fourier series termination ripples (James, 1948). The tests below demonstrate that the proposed approach allows in most cases to separate the influence of these two effects and accurately assign both the local resolution and the local positional uncertainty of atoms.

Our procedure is not limited to crystallographic electron density maps and can be extended to maps of other physical fields, e.g., to the electrostatic scattering potential maps studied by single-particle cryo-EM.

2. Methods

2.1. Limited-resolution atomic images

The electron density distribution and electrostatic scattering potential of an isolated immobile atom in the origin are real-valued spherically symmetric functions. In what follows, we call both ‘atomic density distribution’ and denote by $\rho^{theor}(\mathbf{r})$. Their integral Fourier transform $f(s)$, referred to as the atomic scattering factor, is also real-valued and spherically symmetric. We denote the radial parts of such spherically symmetric functions by an overline, $\rho^{theor}(\mathbf{r}) = \bar{\rho}^{theor}(r)$ and $f(s) = \bar{f}(s)$, where $s = |\mathbf{s}|$ and $r = |\mathbf{r}|$. These radial parts are related to each other by the one-dimensional sine Fourier transforms

$$\bar{f}(s) = \frac{2}{s} \int_0^{\infty} r \bar{\rho}^{theor}(r) \sin 2\pi s r dr, \quad (2)$$

$$\bar{\rho}^{theor}(r) = \frac{2}{r} \int_0^{\infty} s \bar{f}(s) \sin 2\pi s r ds \quad (3)$$

The X-ray and electron scattering factors of all types of atoms and corresponding density distributions are known, as well as their multi-Gaussian approximations (e.g., Doyle and Turner, 1968; Peng, 1999)

$$\bar{f}(s) = \sum_{k=1}^K a_k \exp(-b_k s^2 / 4) \quad (4)$$

Depending on the required accuracy, the number of terms K in these approximations may change (Grosse-Kunstleve et al., 2004) and usually varies from two to five.

Similarly to (1), we define the D -resolution image of the atom by integral (3) calculated within the limits $0 \leq s \leq D^{-1}$.

$$\bar{\rho}^d(r; D) = \frac{2}{r} \int_0^{D^{-1}} s \bar{f}(s) \sin 2\pi s r ds \quad (5)$$

2.2. Shell-approximation to the atomic image

The new concept of the shell approximation to atomic image suggested earlier by the authors (Urzhumtsev and Lunin, 2022a, 2022b; Urzhumtsev et al. 2022; Urzhumtseva et al. 2023) contains three key issues. First, it proposes to interpret heterogeneous maps in structural biology by extended atomic models, traditional parameters of which, such as coordinates and displacement parameters, are completed by point atomic resolutions. Second, atomic images composing such heterogeneous maps are expressed by an analytic function of all these parameters which makes it easy to adjust their values in order to obtain the best fit of the model map to the experimental one. Third, the values of this extended list of parameters can be searched in real space with no direct use of diffraction data. It was shown that for an atom centered at the point \mathbf{r}_{atom} , with scattering factor (4) and with the isotropic atomic displacement parameter B , its image calculated at the resolution D at any point \mathbf{r} of space may be represented as

$$\rho^d(\mathbf{r}; B, D, \mathbf{r}_{atom}) = \frac{4\pi}{3} \sum_{k=1}^K a_k \sum_{m=1}^M \kappa^{(m)} \Omega(\mathbf{r} - \mathbf{r}_{atom}; \mu^{(m)} D, b_k + B + \nu^{(m)} D^2) \quad (6)$$

All terms of this sum are expressed through the same spherically symmetric shell-function of a vector \mathbf{r}

$$\Omega(\mathbf{r}; \mu, \nu) = \frac{1}{|\mathbf{r}| \mu} \sqrt{\frac{1}{4\pi \nu}} \left[\exp\left(-\frac{4\pi^2(|\mathbf{r}| - \mu)^2}{\nu}\right) - \exp\left(-\frac{4\pi^2(|\mathbf{r}| + \mu)^2}{\nu}\right) \right], \quad (7)$$

which is a convolution of a uniform density distribution on the surface of a sphere of radius μ with a Gaussian distribution characterized by the displacement parameter ν . The resolution value D can vary from one atom to another and is associated with the atom, similar to B . All parameters of expression (6), except the atomic coordinates \mathbf{r}_{atom} and values B and D , are known constants. The parameters a_k, b_k define the atomic scattering factor (4) and their values may be found, e.g., in (Peng, 1999) or in (Brown et al., 2006). The values $\mu^{(m)}, \nu^{(m)}, \kappa^{(m)}$ are constants

2.4. Scaling the calculated map

The values to be compared by the least-squares targets such as (8) are often given in different scales. When a linear scaling is acceptable, its parameters κ and ρ^0 , a priori unknown, can be defined for the considered vicinity together with B_{vic}, D_{vic} by minimization of the discrepancy

$$Q(B_{trial}, D_{trial}; \kappa, \rho^0) = \left(\sum_j (\rho_j^{obs} - \kappa (\rho_j^{calc}(B_{trial}, D_{trial}) - \rho^0))^2 / \sum_j (\rho_j^{obs})^2 \right)^{1/2}. \quad (9)$$

of the decomposition of the three-dimensional interference function into a sum of Ω -functions (Urzhumtsev and Lunin, 2022a). An essential feature of decomposition (6–7) is that D is now considered a continuous parameter and not a fixed cutoff.

Formulas (6–7) make it possible to calculate a model map adapted to the errors of the experimental map, provided that the parameters of the atoms are known. They describe morphing the image of an isolated atom when the heterogeneity parameters change. We call B, D as point heterogeneity parameters of the atom to emphasize that they are related to an isolated atom and not to its environment.

2.3. Local map heterogeneity parameters

In a real structure, each map value is a sum of the contributions of several neighboring atoms, which can have different values of point heterogeneity parameters. For a point \mathbf{r}_{ref} , we define its local map heterogeneity parameters as the values which minimize the discrepancy between the map calculated from the model and the experimental one under hypothesis that the point heterogeneity values are the same for all neighboring atoms. In this work, we choose points \mathbf{r}_{ref} coinciding with atomic centers and compare the calculated local map parameters with the point parameters of the heterogeneity of the respective atoms. We formalize this concept as follows.

Let us suppose that an experimental map is defined by its values $\{\rho_j^{obs}\}$ in a grid and $\{\mathbf{r}_{atom,n}\}$ are atomic positions. For a reference point \mathbf{r}_{ref} we define its vicinity $V_{ref}(\mathbf{r}_{ref}, R_{vic})$ as a sphere of a given radius R_{vic} centered in \mathbf{r}_{ref} . Theoretically, all atoms should be taken to calculate the map values inside $V_{ref}(\mathbf{r}_{ref}, R_{vic})$ by (6–7). In practice, functions (6) are assigned to be zero beyond a certain distance R_{cut} from the atomic center, so that only the atoms distanced from \mathbf{r}_{ref} by less than $R_{cut} + R_{vic}$ contribute to the map values. At this stage, we suppose that all atoms contributing to $V_{ref}(\mathbf{r}_{ref}, R_{vic})$ have the same values B_{trial}, D_{trial} of the point heterogeneity parameters, and calculate by (6–7) the values $\rho_j^{calc}(B_{trial}, D_{trial})$ of the model map in the grid nodes of $V_{ref}(\mathbf{r}_{ref}, R_{vic})$. Then we calculate the discrepancy of the model map values from the experimental ones

$$Q(B_{trial}, D_{trial}) = \left(\sum_j (\rho_j^{obs} - \rho_j^{calc}(B_{trial}, D_{trial}))^2 / \sum_j (\rho_j^{obs})^2 \right)^{1/2}. \quad (8)$$

Here the sum is calculated over all grid points which belong to the vicinity $V(\mathbf{r}_{ref}; R_{vic})$. We define the local map heterogeneity parameters $B_{vic}(\mathbf{r}_{ref}), D_{vic}(\mathbf{r}_{ref})$ for the reference point \mathbf{r}_{ref} as B_{trial}, D_{trial} values which minimize this discrepancy. If the reference point coincides with the center of n -th atom as we do it in this work, i.e., when $\mathbf{r}_{ref} = \mathbf{r}_{atom,n}$, we simplify the notations of the heterogeneity values $B_{vic}(\mathbf{r}_{ref}), D_{vic}(\mathbf{r}_{ref})$ as $B_{vic,n}, D_{vic,n}$.

This increases the number of parameters describing the heterogeneity of the experimental map by two individual local scaling coefficients per each vicinity. Eventually, this may overfit the data and lead to instability of the found parameters (Sec. 3.2.2). As a compromise, a two-step procedure has been suggested. In the first run, the map-scaling parameters were determined independently for the vicinity of every reference point. In the second run, the same values of parameters κ, ρ^0 were fixed for all atoms, being taken equal to their average values found from the first run.

Often, the input experimental map $\rho^{obs}(\mathbf{r})$ is given in the σ -scale, with the zero mean value and a unit root-mean-squares deviation. In this case ρ^0 can be estimated as the total scattering content of the cell normalized by the cell volume. With such complementary information, the first run may be performed with the known fixed value of ρ^0 and the only free scale parameter κ .

2.5. Test's protocols

Below, we discuss the results of the tests conducted to find out to what extent the found values of the local map heterogeneity parameters reproduce the point values of these parameters for individual atoms. The input data for each test were:

- a density map for the heterogeneity analysis defined in a grid;
- coordinates of the available atomic model corresponding to the map;
- a set of reference points in the vicinity of which the parameters of local map heterogeneity were searched for; in the tests below, they always corresponded to atomic positions;
- control ('true') values of the atomic heterogeneity parameters for the reference set of atomic positions; these values were obtained by previous experimental projects or were assigned artificially for the goals of the tests; they were never used to determine the parameters of local map heterogeneity but only to analyze the results.

Three protocols of scaling in (9) were used in different runs: fixed κ and ρ^0 values; free κ and ρ^0 ; free κ and fixed ρ^0 .

The method, used in this work, defines the values of the parameters B_{vic}, D_{vic} by a systematic search on a regular grid by parameters B_{trial}, D_{trial} minimizing this discrepancy (9). When necessary, the optimal values of one or two scaling coefficients were determined analytically, since the square of the function (9) is a quadratic function of the parameters κ and $\kappa\rho^0$.

Below, we present the test results for five different density maps. The tests were done with different scaling protocols and the results are shown for different subsets of atoms (e.g., the main chain or the side chains atoms). To simplify the navigation, title of each diagram mentions the analyzed map, the main details of the protocol (if necessary), and a set of atoms for which the results are presented. The program *Pymol* (Schrödinger and DeLano, 2020) was used for illustrations.

The tests were done in increasing order of approaching to the practical case, starting from simulated data, while based on an experimentally solved structure, to fully experimental maps. These latter include both crystallographic protein maps and a cryo-EM map for the ribosome.

2.6. Test objects

2.6.1. A partial and the whole atomic model of the Translation Initiation factor 2

The suggested approach was evaluated first using a part and the whole structure of the core of the Translation Initiation factor 2 protein from *Thermus thermophilus* (IF2). The protein has been crystallized in space group $P2_12_12_1$ with the unit cell dimensions $45.42 \times 61.46 \times 162.40$ Å. The crystal structure (PDB entry 4b3x) has been determined by MAD and refined with the program *phenix.refine* (Afonine et al., 2012) at the resolution of 1.95 Å (Simonetti et al., 2013) with a near complete diffraction data set. The atomic model extracted from the PDB (Burley et al., 2021) contained 2908 atoms of the protein, 220 atoms of water molecules and a glycerol molecule. The protein molecule consists of four domains with a degree of order variable from clearly visible alternative conformations for some residues to highly disordered loops and the C-terminal region. This variability is reflected by the values of its atomic displacement parameters (Fig. 2). These values extracted from the PDB atomic model (B_{atom} below) have been never used for the heterogeneity analysis but only to validate the results of the tests.

To avoid an influence of various experimental, computational, and human errors, we started from the tests with a simulated maps for domain G3 and two simulated maps for the whole protein, namely, a map calculated in the absolute scale and a normalized one. Each such map was calculated as a sum of atomic images, each with its own assigned values B_{atom} , D_{atom} of atomic displacement and atomic image resolution parameters. Then the tests were extended to two types of maps calculated using experimental structure factor magnitudes for IF2 as explained below.

2.6.2. Simulated single particle domain G3 in a virtual unit cell ($G3_{P1}$)

In the first test we considered the domain G3 (83 residues; 682 atoms including 345 main chain atoms N, C $_{\alpha}$, C, O). This domain contains both regular parts and highly disordered loop 357–361 poorly visible in the maps (Fig. 2). Except for the disordered loop, the ADP values $\{B_{atom,n}\}$ of

the main chain atoms vary in the range 20–25 Å² reaching much higher values for side chains (Fig. 2C). The model was placed at the center of a virtual orthogonal unit cell of the size $54.0 \times 54.0 \times 48.0$ Å in the space group P1 ($G3_{P1}$ model). It had no contacts with its translationally-related copies simulating a virtual crystal considered in single-particle studies. The values $\{B_{atom,n}\}$ were extracted from the PDB and all values $\{D_{atom,n}\}$ were assigned equal to 2.0 Å. These values were considered as the control values when analyzing the test results. The map $G3_{P1}$ was calculated in a grid with the step 0.5 Å as the sum of 2.0 Å-resolution images of the model atoms taken in the absolute scale ($e\text{Å}^{-3}$).

2.6.3. Simulated single particle heterogeneous resolution map ($IF2_{VR}$)

For the second series of tests, a single copy of the whole IF2 model was placed at the center of a virtual orthogonal unit cell of the size $80.0 \times 120.0 \times 100.0$ Å in P1 space group. As in the previous test, the molecule had no contacts with its translationally-related copies and the $\{B_{atom,n}\}$ values were taken from the PDB. However, this time the value $D_{atom,n}$ assigned to different atoms varied from 2 Å for the atoms in the central part of the molecule, inside the sphere of the radius 10 Å, to $D_{atom,n} = 5$ Å for the atoms outside the sphere of the radius 40 Å, increasing linearly with the distance to the center in between. The corresponding map was calculated as the sum of atomic images of the respective resolution in the grid with the step 0.5 Å. Depending on the test, the same map was taken in different scales: in the absolute scale or in the σ -scale. This latter simulated the practical situation when the absolute scale of the map is unknown.

2.6.4. IF2 crystallographic maps ($IF2_{obs}$ and $IF2_{\sigma A}$)

Two experimental crystallographic maps of 2 Å resolution were calculated with the coefficients downloaded from the PDB (4b3x). The first map, $IF2_{obs}$, was calculated with the experimentally observed structure factors magnitudes F^{obs} and the phases calculated from the refined atomic model (Simonetti et al., 2013). Differently from the previous maps calculated with simulated data, this map had additional imperfections due to errors in magnitudes and phases. The goal of the test was to estimate to what extent all map distortions can be modeled by only two types of the heterogeneity parameters, $\{B_{vic,n}\}$ and $\{D_{vic,n}\}$, and how well these parameters match the parameters $\{B_{atom,n}\}$ extracted from the PDB and the formal resolution parameters $D_{atom,n} = 2$ Å.

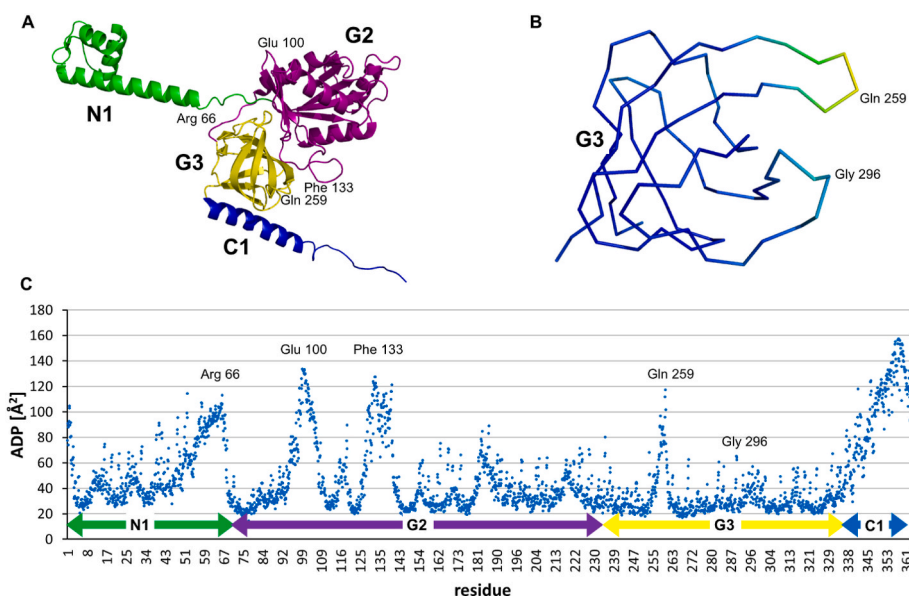


Fig. 2. A. Atomic model of Initiation Factor 2 and its domains. B. Domain G3 backbone colored according to the B -factor. C. Distribution of the B -factor values in the IF2 model.

The second map, $IF2_{\sigma_A}$, was the σ_A -weighted map (Read, 1986) in which the magnitudes are weighted combinations of the experimental and model ones. While both kinds of maps use the same phases, eventually with errors, the σ_A -weighted maps use the modified values of the magnitudes, different from the experimental ones. The goal of such modification is to obtain less noisy maps, easier for their interpretation. However, it is not obvious *a priori* how such modification will influence the parameters which our procedure searches for and if the same two local map heterogeneity parameters are sufficient.

The both maps were calculated at the formal resolution 2.0 Å in the grid with the step 0.5 Å along each coordinate axis.

2.6.5. Cryo-EM structure of human ribosome (HR)

Finally, the proposed approach was tested with an experimental cryo-EM map of the human ribosome, HR (Frechin et al., 2023), kindly provided by the authors. In that original study, the initially found map of an estimated resolution of 2.28 Å was refined and sharpened using the B factor filtering with B equal to -41.11 \AA^2 . This increased the resolution up to approximately 2.18 Å. The local resolution was estimated by the Fourier shell correlation (FSC) with the 0.143 cut-off done by Relion (Zivanov et al., 2018). Map interpretation was done by docking the atomic model of the 80S human ribosome (PDB ID 6QZP) (Wang et al., 2021) into the final maps followed by an automated rigid body fit with Chimera (Pettersen et al., 2004), manual rebuilding with Coot (Emsley et al., 2010) and real space refinement with Phenix (Afonine et al., 2018). This provided refined atomic coordinates and individual $\{B_{atom,n}\}$ and $\{D_{atom,n}\}$ values. Fig. 3 shows the fragment of the available atomic model, Lys 43 – Tyr 73 of the chain Lh, superposed with the experimental map. This map shows unambiguously the main chain atoms and the most of side chains, but not all.

3. Results

3.1. $G3_{p1}$ homogeneous resolution map

The goals of this test were to check the ability of the method to separate the influence of the displacement and resolution parameters on the molecular image in the map, to estimate if the calculated map heterogeneity values B_{vic} , D_{vic} can be used as an approximation to the point atomic heterogeneity values B_{atom} , D_{atom} , and to study an eventual variation of the estimated local resolution parameters D_{vic} for a map of a homogeneous resolution. The map was calculated in the absolute scale ($e\text{\AA}^{-3}$) as the exact image of the G3 domain placed in a virtual unit cell in space group P1 (see Section 2.6.2), using $\{B_{atom,n}\}$ values extracted from the PDB file and with the 2 Å value assigned to all $\{D_{atom,n}\}$. The set of atomic coordinates extracted from the PDB was used to describe both the model atoms $\{r_{atom,n}\}$ and the reference points $\{r_{ref,n}\}$. The trial values of both B_{vic} and D_{vic} varied during the search with the steps 10.0 Å² and 0.5 Å, respectively. The vicinity radius and the cutoff radius of the atomic images were taken as $R_{vic} = 2.1 \text{ \AA}$ and $R_{cut} = 3D_{trial} \text{ \AA}$, depending on the

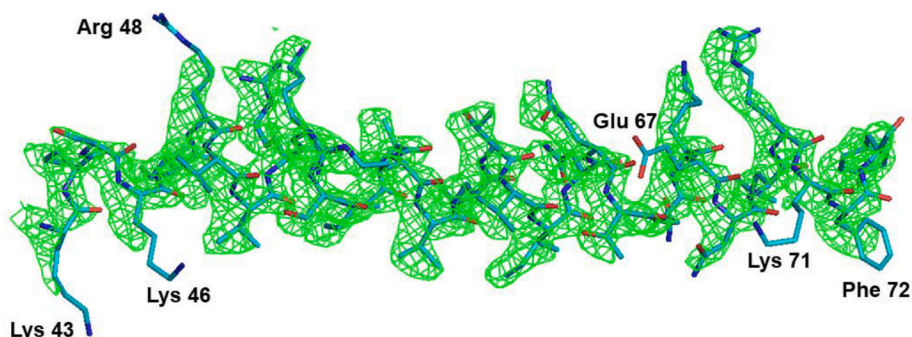


Fig. 3. The fragment Lh Lys 43 – Tyr 73 of the human ribosome superposed with the experimental cryo-EM map.

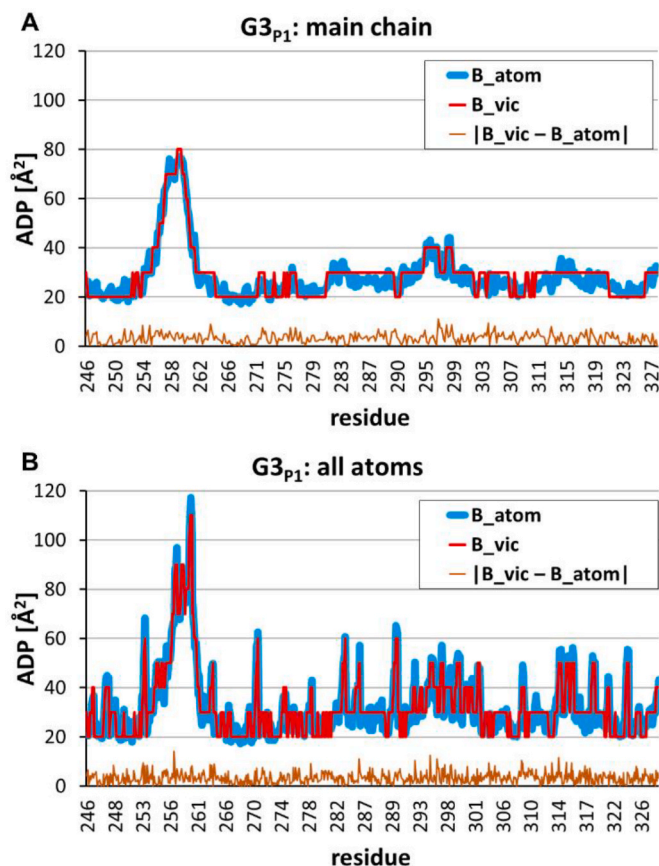


Fig. 4. Results of the heterogeneity analysis of the $G3_{p1}$ map of the 2 Å-resolution. The values B_{vic} were searched with the step of 10 \AA^2 . The B_{vic} values, the control B_{atom} values, and their absolute difference are shown for the main chain atoms (A) and for all atoms (B).

trial resolution value (Urzhumtsev et al., 2022).

Fig. 4 shows the deviation of the $B_{vic,n}$ values, obtained in this test, from the control atomic $B_{atom,n}$ values. For most of atoms the difference between the $B_{vic,n}$ and $B_{atom,n}$ was within the single search step. The mean absolute value of the difference was 3.27 \AA^2 for the whole domain.

For a vast majority of atoms, the D_{vic} value was found to be equal to $D_{atom,n} = 2.0 \text{ \AA}$ used to calculate the map. The only exceptions were observed for a few D_{vic} values equal to 2.5 or 1.5 Å, just neighboring to 2.0 Å. This occurred for 25 atoms from the total number of 682, including 5 main chain atoms from 345, and corresponded to the mean absolute deviation of $D_{vic,n}$ from $D_{atom,n}$ equal to 0.02 Å for all atoms (no plot shown).

This test established two important facts. First, the suggested method

makes it possible to separate the influence of ADP and AIR on the distortion of the atomic image in the map. Second, when being applied to the map of a homogeneous resolution, the given freedom to change the value of the AIR parameter is not taken and, as a rule, the correct value is chosen.

3.2. Heterogeneity analysis of IF2_{VR} maps of a variable resolution

3.2.1. Analysis of the map in the absolute scale

The goal of the next test was to check the ability of the procedure to estimate individual atomic image resolution values for maps of variable resolution. The analyzed map IF2_{VR} was calculated in the absolute scale ($e\text{\AA}^{-3}$) as the exact image of the atomic model with simulated variable atomic image resolution values. The model was placed into a virtual unit cell, the $\{B_{atom,n}\}$ values were extracted from the PDB file, and the $\{D_{atom,n}\}$ values were assigned as described in Sec. 2.6.3. The set of atomic coordinates extracted from the PDB was used both to describe the model atoms $\{r_{atom,n}\}$ and the reference points $\{r_{ref,n}\}$. The trial values of both B_{vic} and D_{vic} were searched with the steps 5.0\AA^2 and 0.2\AA , respectively. The vicinity radius and the atomic image cutoff radius were chosen as $R_{vic} = 2.1 \text{\AA}$ and $R_{cut} = 3D_{trial} \text{\AA}$.

Fig. 5 shows the results of the test. For the most of atoms, the difference between the found D_{vic} and the control D_{atom} values was within a single search step. The mean absolute difference between these values was equal to 0.10\AA for the main chain atoms and 0.15\AA for the side chain atoms. The mean absolute difference between B_{vic} and B_{atom} was 5.40\AA^2 for the main chain atoms and 6.88\AA^2 for the atoms in side chains. However, for some atoms, especially for those with large B_{atom} values or in the low-resolution parts of the map (Fig. 5E), this deviation was larger. It is worthy of noting that in poor defined regions of the map, the found values $D_{vic,n}$ were sometimes larger and sometimes smaller

than the respective $D_{atom,n}$ values. When the found $D_{vic,n} > D_{atom,n}$, the corresponding value $B_{vic,n}$ was smaller than $B_{atom,n}$ (upper left corner in Fig. 5F) to conserve the degree of blurring of the peak in the map. Inversely, for atoms with $D_{vic,n} < D_{atom,n}$ the corresponding value $B_{vic,n}$ was larger than $B_{atom,n}$ (bottom right corner in Fig. 5F).

3.2.2. Heterogeneity analysis of a normalized map

In the test above, both the analyzed map $\rho^{obs}(r)$ and the atomic images for the trial maps $\rho^{calc}(r)$ were calculated in the absolute scale ($e\text{\AA}^{-3}$), the same for both maps, simplifying the search. In practice, maps are usually known in an arbitrary scale often reduced to the σ -scale. As a result, to perform the search for local heterogeneity parameters by minimization of (9), the trial map, calculated initially in the absolute scale, should be linearly scaled, to match the scale of the observed map in (9). The two scaling coefficients κ (dimensionless) and ρ^0 ($e\text{\AA}^{-3}$) may be considered as additional parameters of the search minimizing (9), i.e., four parameters ($B_{vic,n}, D_{vic,n}, \kappa_n, \rho_n^0$) should be found for the vicinity of every reference point (see Methods).

To simulate such situation, a map was calculated in the absolute scale ($e\text{\AA}^{-3}$) from the IF2_{VR} atomic model placed into a virtual unit cell, using the $\{B_{atom,n}\}$ values extracted from the PDB file and with the $\{D_{atom,n}\}$ values defined as described in Section 2.6.3. Then the map was recalculated in the σ -scale with the coefficients $\rho_{exact}^0 = 0.019 e\text{\AA}^{-3}$ and $\kappa_{exact} = 9.741$. The set of atomic coordinates extracted from the PDB was used both to describe the model atoms $\{r_{atom,n}\}$ and the set of reference points $\{r_{ref,n}\}$. The trial values of both B_{vic} and D_{vic} were searched with the steps 5.0\AA^2 and 0.2\AA , respectively. The vicinity radius and the atomic image cutoff radius were taken equal to $R_{vic} = 2.1 \text{\AA}$ and $R_{cut} = 3D_{trial} \text{\AA}$. Figs. 6 and 7 show the results of test performed with different scaling protocols.

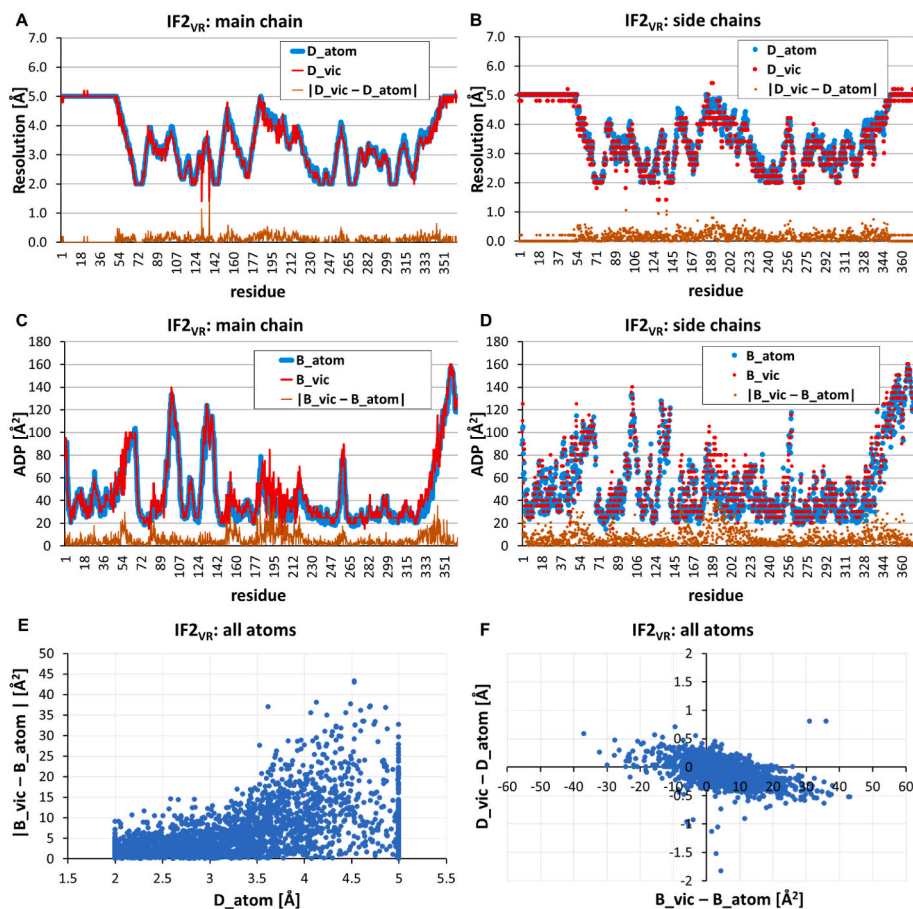


Fig. 5. Results of the heterogeneity analysis of the IF2_{VR} map of a variable resolution. The values B_{vic} were searched with the step of 5\AA^2 , and D_{vic} the with the step of 0.2\AA . A, B) The D_{vic} values, the control D_{atom} values, and their absolute differences for the main chain and side chains atoms. C, D) The B_{vic} values, the control B_{atom} values, and their absolute differences for the main chain and side chain atoms. E). Joint distribution of the absolute deviation of B_{vic} from B_{atom} and D_{atom} value plotted for all atoms; each point in the diagram corresponds to one atom. F) Joint distribution of the deviation of D_{vic} from D_{atom} and the deviation B_{vic} from B_{atom} plotted for all atoms; each point in the diagram corresponds to one atom.

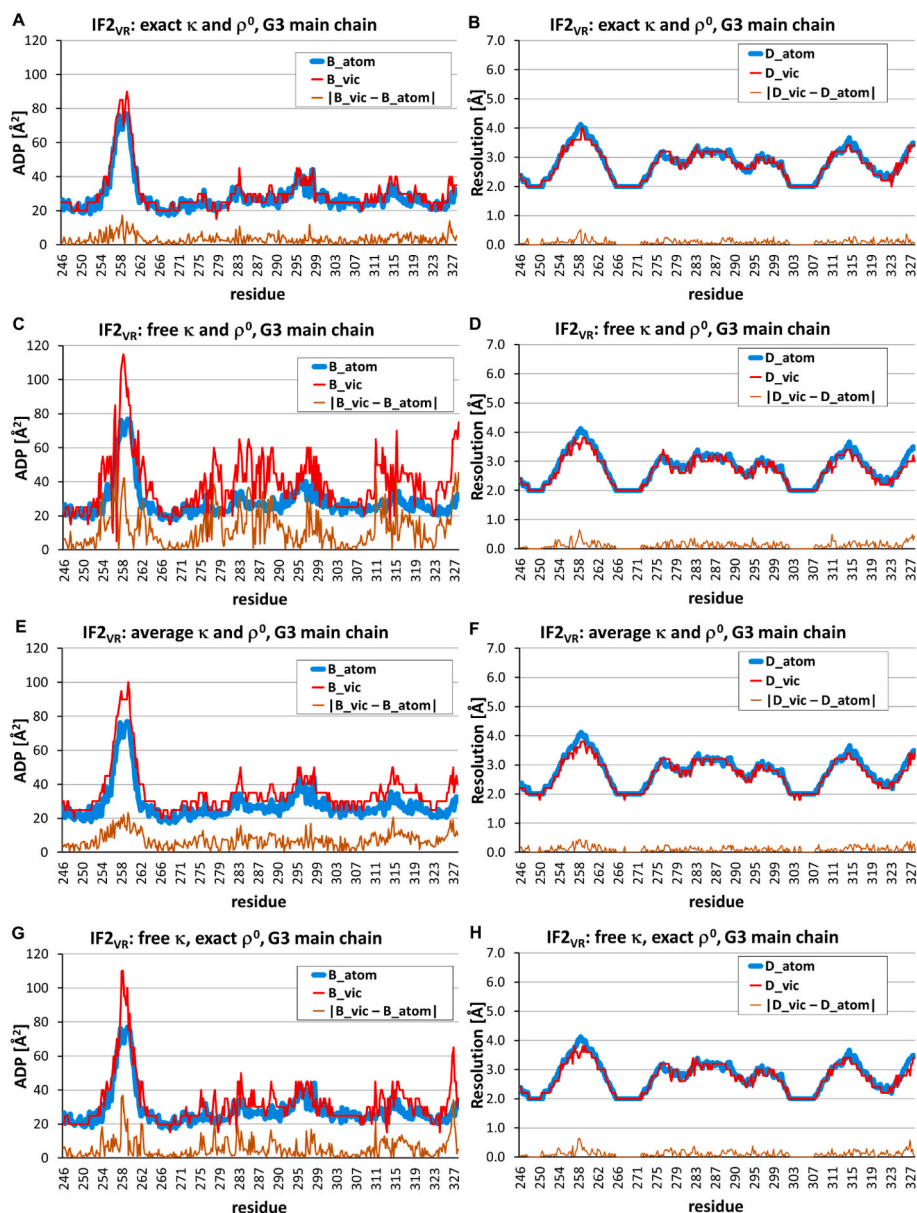


Fig. 6. Results of the heterogeneity analysis of the σ -normalized map for the IF2_{VR} map of a variable resolution using different scaling protocols. The results for the main chain atoms in G3 domain are shown. A, B) The exact scaling values κ and ρ^0 applied in a vicinity of each atom; C, D) scaling values adapted individually in the vicinity of each atom as the average values found from the previous run. E, F) scaling values taken in the vicinity of each atom as the average values found from the previous run. G, H) the exact ρ^0 value fixed for the vicinity of each atom while κ value adapted individually in each vicinity. Left column shows model values B_{atom} , found values B_{vic} , and their absolute deviations. Right column shows the same for the D_{atom} and D_{vic} values.

In the first run, the scaling coefficients were fixed to the exact values $\kappa_n = \kappa_{exact}$, $\rho_n^0 = \rho_{exact}^0$. The results were similar to those from the previous test, that performed in the absolute scale. The mean absolute difference between B_{vic} and B_{atom} was 6.13 \AA^2 for all atoms of the model, and the mean absolute difference between D_{vic} and D_{atom} was 0.12 \AA (Fig. 6A and B). The second test was performed assuming that these scaling coefficients are unknown, and they were searched for each atom independently minimizing (9) (Fig. 6C and D). The results of the second test were worse and illustrated that overparameterization leads to instability in the values of both $B_{vic,n}$ and κ_n (Figs. 6C and 7A). The mean absolute difference between B_{vic} and B_{atom} has increased to 14.68 \AA^2 . Surprisingly, the difference between D values remained at the same level of 0.13 \AA as previously. Then the values κ_n, ρ_n^0 found for all atoms were averaged, resulting in $\kappa_{ave,1} = 10.373$ and $\rho_{ave,1}^0 = 0.035 e\text{\AA}^{-3}$. These average values were taken as fixed scaling coefficients in the next run (Fig. 6E and F). Now the absolute difference between the control and determined parameter values was 14.96 \AA^2 for B and 0.24 \AA for D . As an alternative scaling protocol, we fixed the ρ_n^0 values making them equal to the value calculated analytically from the atomic content of the virtual

crystal and equal to the Q_{exact}^0 value, used for the map normalization. The run performed with such ρ_n^0 values (Fig. 6G and H), resulted in the absolute difference for map and atomic B and D values equal to 9.92 \AA^2 and 0.13 \AA , respectively. The κ_n values varied much less (Fig. 7B) and their average $\kappa_{ave,2} = 9.739$ was very close to the exact $\kappa_{exact} = 9.741$ value used in the map normalization. The B_{vic} and D_{vic} found with $\kappa_{ave,2}, \rho_{exact}^0$ were as accurate as in the test with the exact scaling coefficients (Fig. 6A and B).

To check the role of the search step, the calculation was repeated with fixed values of the scaling coefficients $\kappa_{ave,2}, \rho_{exact}^0$ and the steps of the trial values increased to 10.0 \AA^2 for B_{vic} and to 0.5 \AA for D_{vic} . The obtained mean absolute difference between the map and atoms heterogeneity values B and D for all atoms in G3 domain became 5.27 \AA^2 and 0.16 \AA . This shows that such coarser steps 10.0 \AA^2 and 0.5 \AA are sufficient to estimate the values of local heterogeneity parameters.

3.3. Heterogeneity analysis of IF2 crystallographic maps

3.3.1. Unweighted map

Finally, the developed approach was applied to two crystallographic

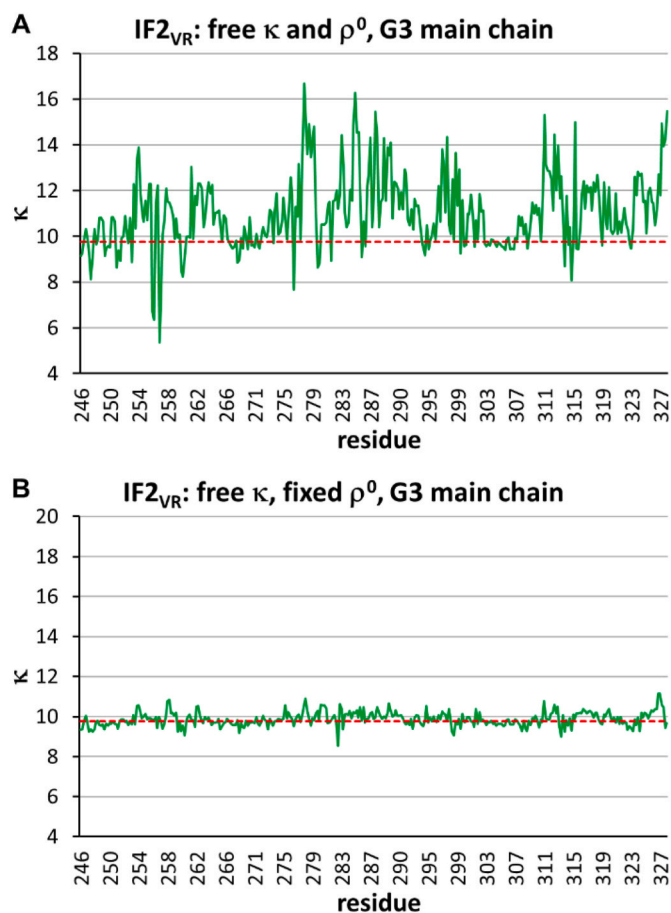


Fig. 7. The value of the individual scaling factor κ_n in the vicinity of the main-chain atoms of the G3 domain of IF2_{VR}; the values are found from the analysis of the σ -normalized map of a variable resolution. A) Search with variable κ and ρ^0 values; B) search with variable κ and fixed ρ^0 value equal to the exact value. Dashed lines show the exact parameter value known for this test case.

maps corresponding to the crystal structure of IF2 for which a near complete set of structure factors and the model refined at resolution of 1.95 Å were available. The first map was calculated as the Fourier synthesis (1) with the coefficients $F^{obs}(s)\exp[i\varphi^{calc}(s)]$, combining the experimentally obtained magnitudes $F^{obs}(s)$ with the phases $\varphi^{calc}(s)$ calculated from the model, both available from the PDB. All structure factors of the resolution up to 2.0 Å were included into the synthesis calculation (Section 2.6.4).

First, the analysis was performed with the variable map-scaling parameters κ and ρ^0 , which means that in each vicinity the calculated density was scaled to the observed one with its individual coefficients. Expectedly from the test calculations, such search has resulted in an unstable behavior of the scaling coefficients leading to a relatively large deviation of some found B_{vic} values from the respective model ADP values B_{atom} (Fig. 8). Nevertheless, the mean absolute deviation was not so large and constituted 13.97 Å² for all atoms. The mean absolute deviation of D_{vic} from the actual value $D_{atom} = 2\text{Å}$, the same for all atoms, was 0.149 Å for the main chain and 0.180 Å for all atoms. Averaging the found scaling parameters κ and ρ^0 over the main chain atoms of the relatively stable G3 domain resulted in the values 4.08 and 0.347 eÅ⁻³. The latter value is quite close to the estimate $F_{000}/V_{cell} \approx 0.363\text{ eÅ}^{-3}$ calculated from the PDB model content.

Then, the procedure was repeated taking both the parameters κ and ρ^0 fixed, equal to the mean values found from the first run. Now, the estimated resolution values D_{vic} coincided with the formal value of 2.0 Å for the most of atoms (Fig. 9 C, D), with the mean absolute deviation equal to 0.29 Å. The deviation of the B_{vic} values from the control ones was reduced to 7.80 Å². However, while the mean deviation values were small comparatively to the search steps 0.5 Å and 10.0 Å², the errors for some atoms were significant (Fig. 9).

3.3.2. Standard σ_A -weighted map

The second experimentally-based IF2 crystallographic map was the standard σ_A -weighted one (Read, 1986) with the coefficients calculated by *phenix.refine* and available in the PDB. Similar to the previous calculations, the search for the B_{vic} , D_{vic} parameters was performed in two iterations but, differently to the analysis of the unweighted map (Sec.3.3.1), now we fixed ρ^0 equal to the value $\rho_{est}^0 = 0.363\text{ eÅ}^{-3}$ calculated from the PDB model content, while the parameter κ was

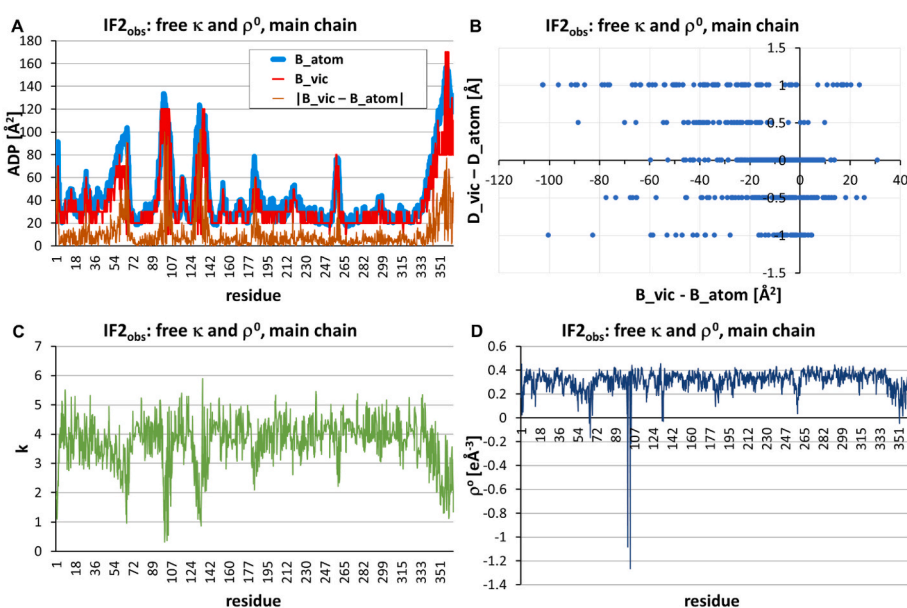


Fig. 8. Heterogeneity analysis of the 2 Å-resolution Fourier synthesis for IF2 structure calculated with the coefficients (F^{obs} , φ^{calc}). The results are shown for the main chain atoms. The run was performed with the variable scaling values. A) The values B_{vic} , B_{atom} , and their absolute difference. B) The joint distribution of the deviations $D_{vic} - D_{atom}$ and $B_{vic} - B_{atom}$. C) The found scaling factors κ and D) The found scaling values ρ^0 .

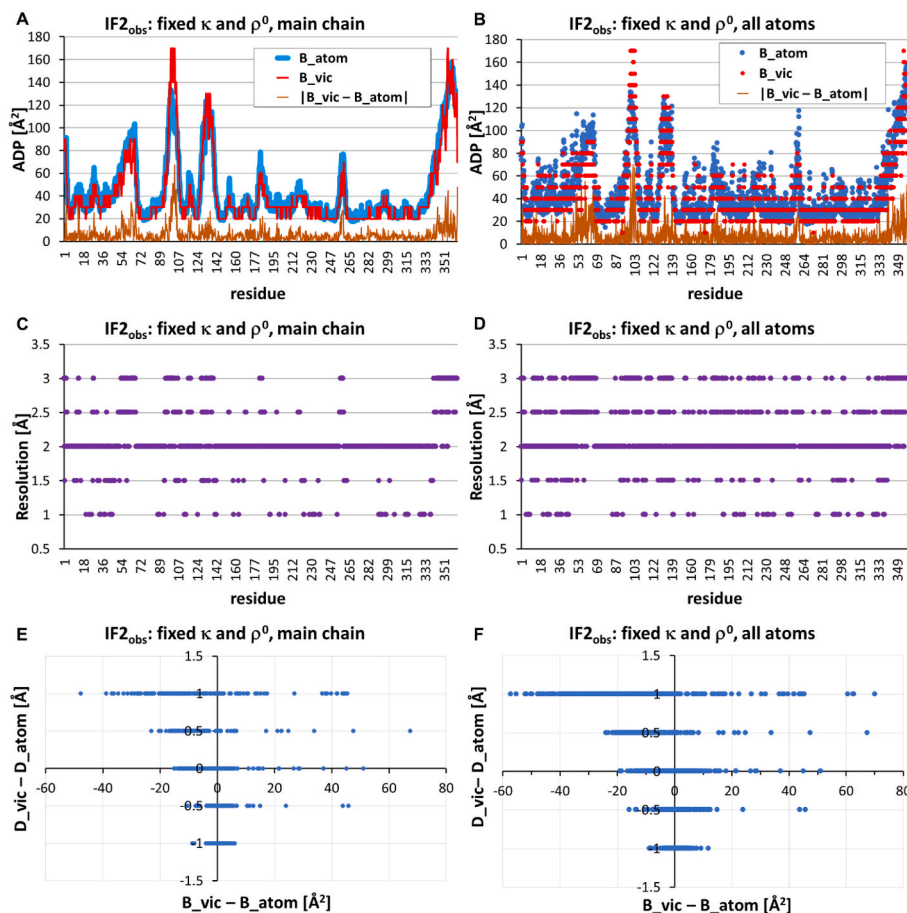


Fig. 9. Heterogeneity analysis of the IF2 2 Å-resolution Fourier synthesis, calculated with the coefficients (F^{obs}, ρ^{calc}). The analysis was done with fixed values of the scaling parameters κ and ρ^0 , taken in the vicinity of each atom as the average values found from the previous run. A, B) The values B_{vic} , B_{atom} , and their absolute differences. C, D) The found D_{vic} values. E, F) The joint distribution of the deviations $D_{vic} - D_{atom}$ and $B_{vic} - B_{atom}$.

considered as free and searched for in the first run. The deviations of its found values from the mean value clearly correlated with the values of the score function Q (9) (Fig. 10). By this reason, the average κ -value to be used in the second run was calculated considering only the main-chain atoms with $Q < 0.2$ and resulted in $\kappa_{ave} = 4.43$. In the second run the values of the scale parameters were fixed and equal to κ_{ave} and ρ_{est}^0 values. Fig. 11 shows results of the second run for the atoms of G3 domain. For most of them the values of B_{vic} , D_{vic} reproduced the values of the corresponding parameters of the atoms as accurately as in the test with the simulated data (Fig. 7G). The number of atoms with the D_{vic} value different from the formal synthesis resolution 2 Å, was 37 from 345 main chain atoms, and 140 from all 682 atoms. The mean absolute deviation from the formal resolution value 2.0 Å was 0.20 Å for all atoms of the G3 domain, and the mean absolute deviation of B -value was 5.14 Å². The plot of the obtained values of the score function (9) (Fig. 11 C) reflects anomalies in the defined B_{vic} , D_{vic} values which may be caused by insufficient quality of the respective map regions and of the atomic model built there.

3.4. Heterogeneity analysis of the cryo-EM ribosome map

The proposed approach could be applied to the maps obtain not necessary by crystallography but by other techniques, in particular, by cryo-EM. However, refinement of atomic models against cryo-EM data is not yet so well-established as in crystallography, and its results should be taken with some caution. In particular, cryo-EM maps are often sharpened and postprocessed, so the estimated ADP values may have no clear physical meaning and may vary in the range different from that

usual for crystallography. Also, the resolution defined from the FSC analysis determines the reproducibility of the result (precision) rather than the visual quality of the map and may differ from the crystallographic meaning of this term (Penczek, 2010; Afonine et al., 2018). For the goals of this project, we used the ribosome experimental data and the respective model as described in Section 2.6.5.

Similar to the previously described cases, the evaluation of the B_{vic} , D_{vic} parameters for the atomic model was performed in two iterations. In the first run, the scaling parameters κ , ρ^0 were considered as variable and defined individually in the vicinity of each atom together with B_{vic} , D_{vic} . Then, the scaling parameters defined for main chain atoms were averaged and these average values were fixed and used for the second iteration. Atomic images were calculated using the 4-Gaussian approximation to the atomic scattering factors (Peng, 1999). The radius of the vicinity in these tests was taken equal to 4 Å. The steps in B_{trial} , D_{trial} values were 5 Å² and 0.25 Å, respectively. The values found by Phenix (Afonine et al., 2018) and Relion (Zivanov et al., 2018) were considered as the control values $B_{atom,n}$, $D_{atom,n}$.

Fig. 12 shows that for the main chain atoms and the most of side chains atoms the estimated resolution D_{vic} is close to the values D_{atom} obtained with Relion. The exception are the side chains for which the density in experimental map is poor (Lys 43, Arg 48, Gln 65, Glu 67, Lys 71).

The found B_{vic} values for the main chain and most of side chain atoms vary around 20 Å², the value usual for crystallographic atomic models obtained at 2 Å resolution. They are different from excessively low values B_{atom} defined by Phenix. For the six side chains with poorly defined density in the experimental map, the same as above plus Lys 46,

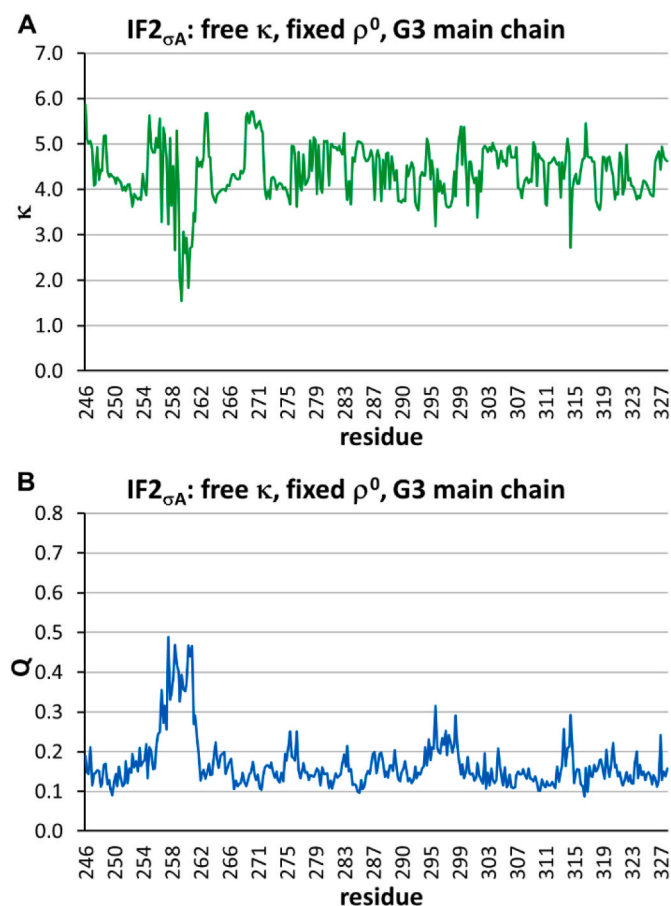


Fig. 10. Heterogeneity analysis of σ_A -weighted map for G3 domain main chain performed with a variable coefficient κ and the fixed ρ^0 value, estimated from the PDB model content. A. Variation of κ_n along the chain. B. Variation of the score function (9) value along the chain.

the found B_{vic} values are much larger. The discrepancy (9) values corresponding to the optimal choice of B_{vic}, D_{vic} reflect this tendency revealing larger Q-values for the atoms poorly defined in the map.

Fig. 13 shows a fragment of the experimental map (Fig. 13, A), and the same fragment of the map calculated with the atomic parameter values provided by *Relion* and *Phenix* (Fig. 13, B), and alternatively of the map calculated with the B_{vic}, D_{vic} values found by the method suggested in this work (Fig. 13, C). The map calculated with the *Relion* and *Phenix* parameters does not reflect the actual quality of experimental map, e.g., for residues Glu 65, Glu 67, Lys 71. Instead, the parameters values B_{vic}, D_{vic} obtained with the approach developed here allow reproducing the experimental map much better (Fig. 13 C, D).

It is worthy of noting that the atomic model used in this test is not the ideal model corresponding to the experimental map. Eventual inaccuracies in the atomic positions can be revealed by comparison of the experimental map with the image calculated as (6–7) with the parameters B_{vic}, D_{vic} defined by minimization of (9). Fig. 14 gives an example of such comparison suggesting the developed approach to be a component of future real-space refinement procedures allowing to improve atomic models further.

4. Discussion

Experimental maps in structural biology usually differ from the respective theoretical distributions due to various reasons. In this paper we address to two important reasons, namely a positional disorder of atomic centers and a limited resolution with which images of atoms appear in experimental maps. These two characteristics may be het-

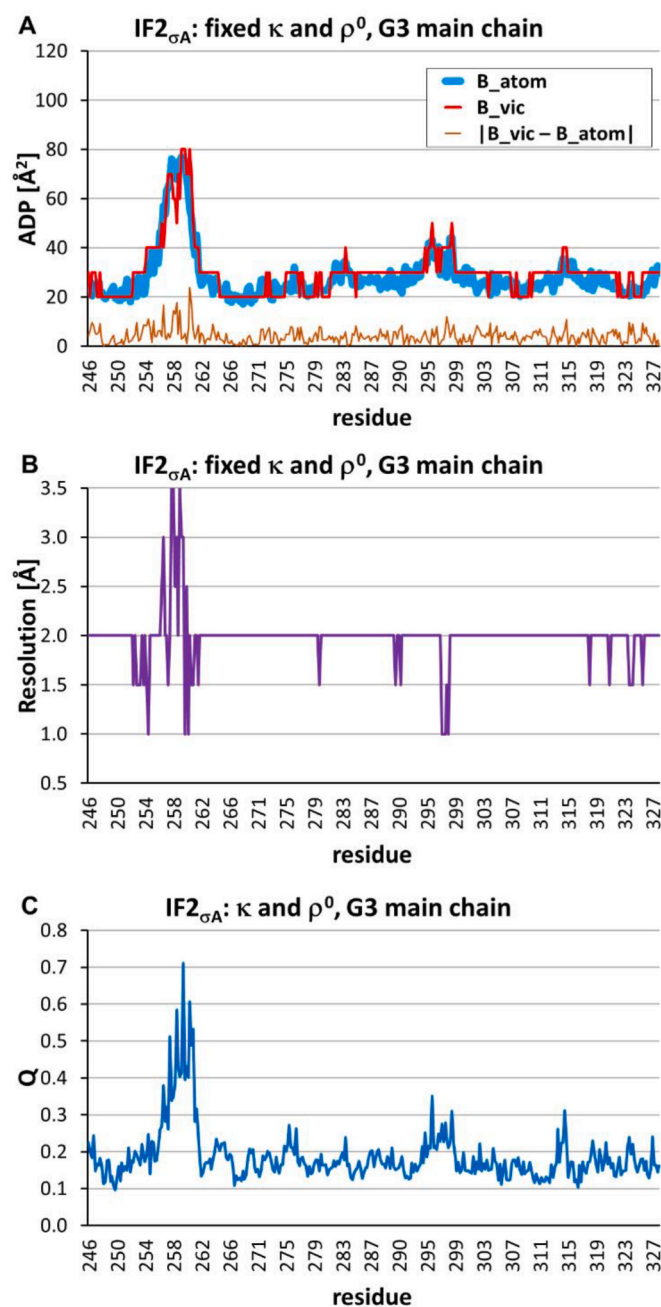


Fig. 11. Heterogeneity analysis of σ_A -weighted map for IF2 with the fixed κ_{ave} and ρ_{est}^0 coefficients. The results are shown for the G3 main chain atoms. A. Variation of the B_{vic}, B_{atom} values along the chain and their absolute difference. B. Variation of the D_{vic} value along the chain C. Variation of the score function (9) value along the chain.

erogeneous varying from one region to another. Eventually they may be attributed individually for every atom of the object as atomic displacement parameter B_{atom} and atomic image resolution D_{atom} . Recently we have suggested a method to describe atomic images of a limited resolution by shell-functions, that allows one to calculate heterogeneous density maps (Urzhumtsev and Lunin, 2022a) as sums of images of isolated atoms expressed analytically in terms of heterogeneity parameters.

In this article, we report the results of our attempts to develop an inverse procedure, i.e., to annotate heterogeneity of an experimental density maps in terms of point heterogeneity parameters of all atoms. In a future, this could be done by a multidimensional search in the space of

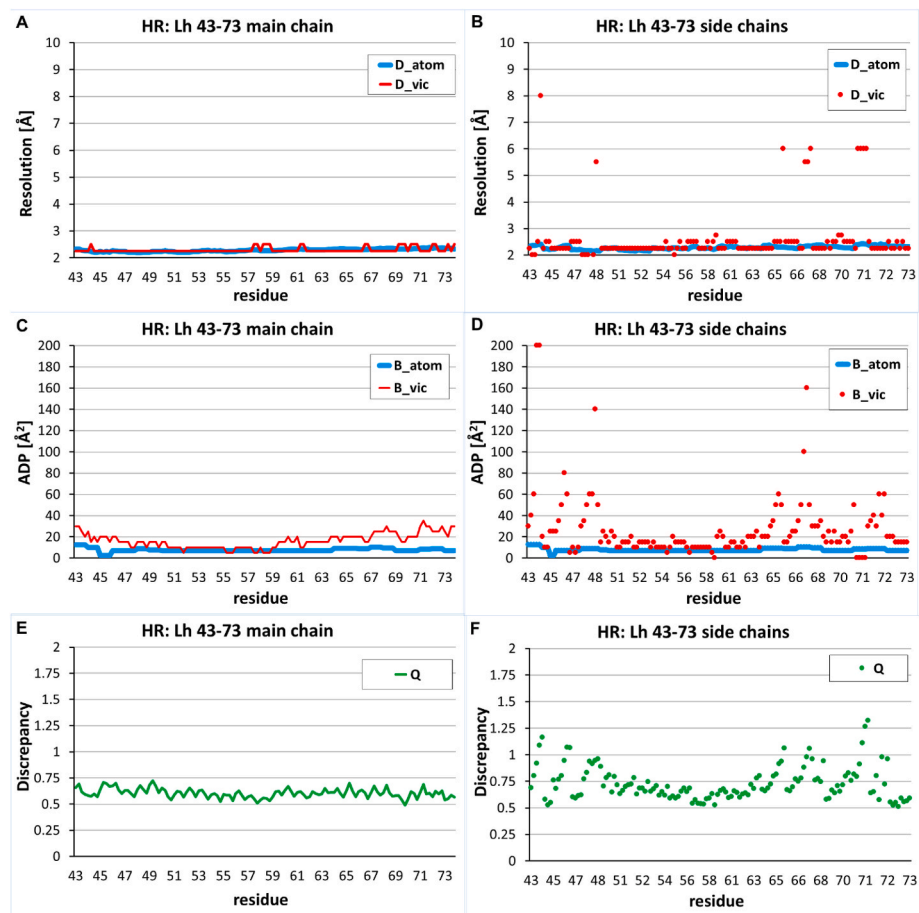


Fig. 12. Results of heterogeneity analysis of the human ribosome cryo-EM map performed for Lys43-Tyr73 fragment (in chain Lh) shown for the main chain (left) and the side chain (right) atoms.

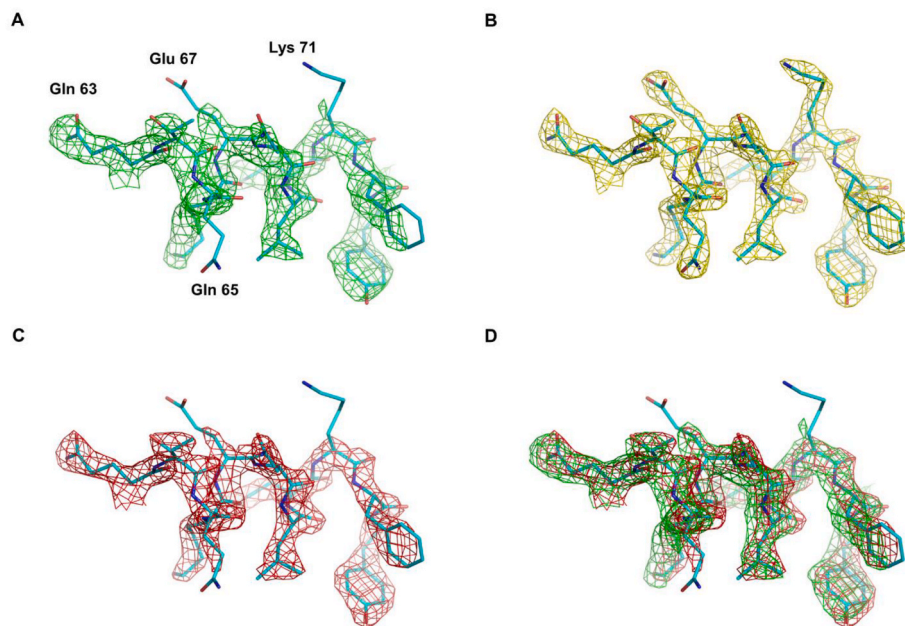


Fig. 13. Maps showing the Lh Lys43-Tyr73 ribosome fragment superposed with the atomic model. A) The experimental cryo-EM map. B) The map calculated with the B_{atom} , D_{atom} parameter values defined with *Relion* and *Phenix*. C) The map calculated with the B_{vic} , D_{vic} parameter values, defined by minimization of discrepancy (9). D) Superposition of maps from A and C. The cut-off value in each map was chosen to display the equal specific volume of the selected regions ($0.15 \text{ \AA}^3 \text{Da}^{-1}$).

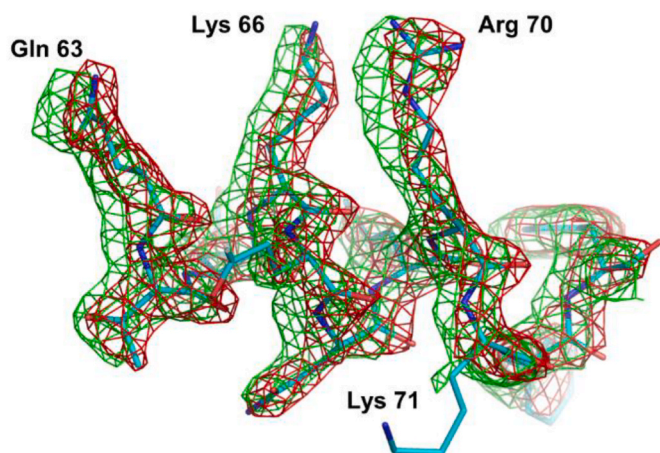


Fig. 14. A fragment of the atomic model of a ribosome superposed with the experimental cryo-EM map (green) and with the model map (red) calculated with the current values of the atomic parameters. The revealed systematic difference suggests to correct the position of some atoms. The cut-off in both maps was chosen to display the equal specific volume of the selected regions ($0.15 \text{ \AA}^3 \text{ Da}^{-1}$). (For interpretation of the references to color in this figure legend, the reader is referred to the Web version of this article.)

all atomic heterogeneity parameters, minimizing the discrepancy between the calculated and experimental maps. At the moment, we have proposed a simplified approach that allows one to obtain estimates of these parameters locally, processing atom by atom. The problem of such search is that in every point in space the value of the density is a sum of several atomic contributions, mixing up parameters of neighboring atoms in the discrepancy function. To overcome this problem, we introduce the concept of the local map heterogeneity parameters B_{vic} , D_{vic} assuming temporary that in a vicinity of a given point all atoms contributing to the map have the same point heterogeneity parameters. The values B_{vic} , D_{vic} may be assumed a ‘consensus’ values of individual parameters of neighboring atoms. These map heterogeneity values may be calculated locally for each point in space and produce some kind of annotation of the heterogeneity of the given density map. One should distinguish between then map heterogeneity parameters B_{vic} , D_{vic} , calculated from the map values around the center of an atom, and the point parameters B_{atom} , D_{atom} with which this particular atom contributes to the map. Therefore, the first goal of our study was to verify whether the calculated B_{vic} , D_{vic} values may serve as estimates for the point heterogeneity parameters. Our test, conducted for simulated maps, where the only present types of distortions were positional disorder and the loss of resolution (Sec. 3.1, 3.2), gave the positive answer for a vast majority of atoms. The ambiguity of the definition of parameters was manifested only for highly disordered low-resolution parts of the maps (Fig. 5).

The experimental methods of structural biology such as X-ray and neutron crystallography and single particle cryo-EM, do not report B_{vic} , D_{vic} directly. Moreover, experimental maps are distorted also by the reasons other than the positional disorder and loss of resolution. Therefore, the second goal of our tests, performed this time with experimental maps (Sec. 3.3, 3.4), was to find to what extent B_{vic} , D_{vic} calculated with the proposed method reproduce the values of atomic displacement parameter B_{XR} obtained by crystallographic refinement programs and D_{EM} resolution estimated by the Fourier Shell Correlation function in cryo-EM.

For experimental X-ray maps, the difference between B_{vic} values and B_{XR} , extracted from PDB, did not exceed those in the tests with simulated maps (Figs. 10 A and 11 A vs Fig. 4A). This suggests both that the values B_{vic} are a reasonable approximation to the crystallographic displacement parameters B_{XR} , and that the additional distortions inherent to the map do not significantly affect the accuracy of this approximation. The D_{vic}

value in different points coincided with the formal resolution of Fourier syntheses for most atoms, or was only slightly different from it (Fig. 11 B). The exceptions were poor defined regions in the map, where the variation of resolution improved the correspondence between the calculate and experimental maps. Surprisingly, in all our tests, the resolution was estimated more accurately than the ADP values (Fig. 6). We assume that this can be explained by the fact that changing the resolution shifts the positions of the ripples, which may be more important information than the degree of blurring of the density peaks.

For well-defined regions of the analyzed cryo-EM map, the found D_{vic} values were close to the D_{EM} values annotated by *Relion* program (Fig. 12 A, B). Nevertheless, for some side chains poor defined in the map D_{vic} differed significantly from the D_{EM} values, suggesting much lower resolution (Fig. 12 B). The calculation of fragments of the model map with $\{B_{EM}, D_{EM}\}$ replaced by $\{B_{vic}, D_{vic}\}$ showed that using the new values of the parameters allows one to reproduce the experimental map better (Fig. 13). Concerning the displacement parameters, our approach has resulted in usual-scale values B_{vic} which are larger than extremely small values B_{EM} annotated after previous refinement against experimental cryo-EM map (Fig. 12 C, D). There are two possible explanations. Firstly, EM-maps are subjected to additional processing, for example, sharpening, and to describe such maps, atomic displacement parameters should be also reduced. Secondly, the refinement against cryo-EM maps is not yet a well-established procedure requiring its further development.

The proposed approach to estimate heterogeneity of maps uses available values of the atomic coordinates. If these coordinates contain errors, then a map corresponding to the model calculated with the found heterogeneity parameters can reveal errors in the location of atoms (Fig. 14). Inversely, incorrect atomic position may lead to errors in estimated B_{vic} , D_{vic} values. A joint refinement of all parameters may be an option in future.

A significant problem when working with experimental maps is scaling, i.e., bringing the map calculated from the model to the scale of the experimental map by a linear transformation $\rho^{new} = \kappa(\rho^{model} - \rho^0)$. The proposed approach to search for B_{vic} , D_{vic} has a local character, i.e., each calculation is done independently in a small vicinity of a point. An attempt to determine the optimal scaling coefficients also locally, based on the analysis of the map values only inside this vicinity, can lead to a sharp variation of the values of the scaling parameters between neighboring vicinities (Figs. 7A and 8 C, D, Fig. 10A). This in turn may results in errors in the determined heterogeneity parameters. The behavior of parameter κ changes drastically if the parameter ρ^0 is fixed for all vicinities (Fig. 7) being estimated as

$$\rho_{est}^0 = \left[\rho_{sol} V_{sol} + \sum_n \bar{f}_n(0) \right] / V_{cell} \quad (10)$$

Here $\bar{f}_n(0)$ are atomic scattering factors (2) or (4) in the origin, V_{cell} is the unit cell volume, the sum is calculated over all atoms in the unit cell and the complementary term is designed to consider the bulk solvent contribution, when exists, with ρ_{sol} , V_{sol} being the mean solvent density and the volume of the solvent region.

In the suggested approach, for every atom we introduce an atomic image resolution as an additional variable parameter. This increases the number of parameters to describe an experimental map and raises the question if this indeed improves the model with no data overfitting. Especially this concerns cryo-EM maps when Fourier resolution cutoff is not explicitly used. Nevertheless, cryo-EM maps also miss a number of higher-resolution Fourier harmonics due to experimental features and image processing. As it follows from the tests performed, the suggested approach does not use the additional freedom when it is not necessary. For test and experimental Fourier syntheses of a fixed resolution, the found D_{vic} values coincide with the formal resolution of Fourier syntheses for a vast majority of atoms. On the other hand, when being applied to test syntheses of known inhomogeneous resolution, the pro-

cedure determines properly different D_{vic} values. For cryo-EM maps, the procedure determines different D_{vic} values for different regions in the map accordingly to the map quality and improves the correspondence of the model map to the experimental one. Altogether, this advocates for usefulness of D_{vic} parameters in calculation of model maps both for crystallographic and cryo-EM studies.

The results obtained in the reported work prove the feasibility of the solution of the inverse problem of the decomposition of density maps, *i. e.*, a possibility to recover the values of the parameters of two principal phenomena which affect the molecular images, namely the local resolution and the local positional uncertainties. For well-ordered regions, these parameters may be adjusted by refinement programs. For poorly-ordered regions various acceptable combinations of the respective parameters lead to similar density maps and any of these combinations can be taken. This aspect of the procedure, as well as modeling of more tiny effects such as an anisotropic disorder, require a further analysis which is in progress.

5. Conclusions

The proposed approach allows to annotate the heterogeneous imperfections of experimental maps obtained in structural biology. Within this approach, the heterogeneity is expressed in terms of variation, from one point to another, of the local atomic displacement and local resolution parameters. The developed real space procedure, based on the shell approximation of atomic images, allows appropriate estimates of these parameters, and reproduces properly the resolution value when applied to maps of a homogeneous resolution. For well-ordered parts of the structure, the estimates of the atomic displacement parameters determined by the proposed method are close to those found by reciprocal space refinement. For less ordered parts, which are poorly represented in an experimental map, a simultaneous correction of displacement and resolution parameters presents an alternative description of heterogeneity and allows one to get a better local correspondence of the calculated and the observed maps.

CRedit authorship contribution statement

Vladimir Y. Lunin: Conceptualization, Methodology, Software, Writing – original draft. **Natalia L. Lunina:** Data curation, Software, Visualization. **Alexandre G. Urzhumtsev:** Conceptualization, Methodology, Software, Writing – original draft.

Declaration of competing interest

The authors declare that they have no known competing financial interests or personal relationships that could have appeared to influence the work reported in this paper.

Data availability

The authors do not have permission to share data.

Acknowledgements

We thank L.M. Urzhumtseva for help with computing, tests, and program development. AU acknowledges Instruct-ERIC and the French Infrastructure for Integrated Structural Biology FRISBI [ANR-10-INBS-05].

This research did not receive any specific grant from funding agencies in the public, commercial, or not-for-profit sectors.

References

Afonine, P.V., Lunin, V.Y., Muzet, N., Urzhumtsev, A., 2004. On the possibility of the observation of valence electron density for individual bonds in proteins in

- conventional difference maps. *Acta Crystallogr. D60*, 260–274. <https://doi.org/10.1107/S0907444903026209>.
- Afonine, P.V., Echols, N., Grosse-Kunstleve, R.W., Headd, J.J., Moriarty, N.W., Mustyakimov, M., Terwilliger, T., Urzhumtsev, A., Zwart, P.H., Adams, P.D., 2012. Toward automated crystallographic structure refinement with phenix.refine. *Acta Crystallogr. D68*, 352–367. <https://doi.org/10.1107/S0907444912001308>.
- Afonine, P.V., Klaholz, B.P., Moriarty, N.W., Poon, B.K., Sobolev, O.V., Terwilliger, T.C., Adams, P.D., Urzhumtsev, A., 2018. New tools for the analysis and validation of Cryo-EM maps and atomic models. *Acta Crystallogr. D74*, 814–840. <https://doi.org/10.1107/S2059798318009324>.
- Bragg, W.H., 1920. The intensity of X-ray reflection in diamonds. *Proc. Phys. Sci. London* 33, 304–311. <https://doi.org/10.1088/1478-7814/33/1/331>.
- Brown, P.J., Fox, A.G., Maslen, E.N., O'Keefe, M.A., Willis, B.T.M., 2006. Intensity of diffracted intensities. In: Prince, E. (Ed.), *International Tables for X-Ray Crystallography*, C. Dordrecht: Springer, Dordrecht, The Netherlands, pp. 554–595 ch. 6.1.
- Burley, S.K., et al., 2021. RCSB Protein Data Bank: powerful new tools for exploring 3D structures of biological macromolecules for basic and applied research and education in fundamental biology, biomedicine, biotechnology, bioengineering and energy sciences. *Nucleic Acids Res.* 8, D437–D451. <https://doi.org/10.1093/nar/gkaa1038>.
- Cardone, G., Heymann, J.B., Steven, A.C., 2013. One number does not fit all: mapping local variations in resolution in cryo-EM reconstructions. *J. Struct. Biol.* 184, 226–236. <https://doi.org/10.1016/j.jsb.2013.08.002>.
- Chapman, M.S., 1995. Restraint real-space macromolecular atomic refinement using a new resolution-dependent electron-density function. *Acta Crystallogr. A51*, 69–80. <https://doi.org/10.1107/S0108767394007130>.
- Chapman, M.S., Trzynka, A., Chapman, B.K., 2013. Atomic modeling of cryo-electron microscopy reconstructions – joint refinement of model and imaging parameters. *J. Struct. Biol.* 182, 10–21. <https://doi.org/10.1016/j.jsb.2013.01.003>.
- Cruickshank, D.W.J., 1999. Remarks about protein structure precision. *Acta Crystallogr. D55*, 583–601. <https://doi.org/10.1107/S0907444998012645>.
- Diamond, R., 1971. A real-space procedure for proteins. *Acta Crystallogr. A27*, 436–451. <https://doi.org/10.1107/S0567739471000986>.
- DiMaio, F., Song, Y., Li, X., Brunner, M.J., Xu, C., Conticello, V., Egelman, E., Marlovits, T., Cheng, Y., Baker, D., 2015. Atomic-accuracy models from 4.5-Å cryo-electron microscopy data with density-guided iterative local refinement. *Nat. Methods* 12, 361–365. <https://doi.org/10.1038/nmeth.3286>.
- Doyle, P.A., Turner, P.S., 1968. Relativistic Hartree-Fock X-ray and electron scattering factors. *Acta Crystallogr. A24*, 390–397. <https://doi.org/10.1107/S0567739468000756>.
- Emsley, P., Lohkamp, B., Scott, W.G., Cowtan, K., 2010. Features and development of Coot. *Acta Crystallogr. D66*, 486–501. <https://doi.org/10.1107/S0907444910007493>.
- Evans, P.R., Murshudov, G.N., 2013. How good are my data and what is the resolution? *Acta Crystallogr. D69*, 1204–1214. <https://doi.org/10.1107/S0907444913000061>.
- Frechin, L., Holvec, S., von Loeffelholz, O., Hazemann, I., Klaholz, B.P., 2023. High-resolution cryo-EM performance comparison of two latest-generation cryo electron microscopes on the human ribosome. *J. Struct. Biol.*, 107905 <https://doi.org/10.1016/j.jsb.2022.107905>.
- Grosse-Kunstleve, R.W., Sauter, N.K., Adams, P.D., 2004. Cctbx news. *Newsletter of the IUCr Commission on Crystallographic Computing* 3, 22–31.
- Gurusaran, M., Shankar, M., Nagarajan, R., Helliwell, J.R., Sekar, K., 2014. Do we see what we should see? Describing non-covalent interactions in protein structures including precision. *IUCr J*, 1, 74–81. <https://doi.org/10.1107/S2052252513031485>.
- James, R.W., 1948. False detail in three-dimensional Fourier representations of crystal structures. *Acta Crystallogr. A1*, 132–134. <https://doi.org/10.1107/S0365110X48000351>.
- Karplus, P.A., Diederichs, K., 2012. Linking crystallographic model and data quality. *Science* 336, 1030–1033. <https://www.science.org/doi/10.1126/science.1218231>.
- Kucukelbir, A., Sigworth, F.J., Tagare, H.D., 2014. Quantifying the local resolution of cryo-EM density maps. *Nat. Methods* 11, 63–65. <https://doi.org/10.1038/nmeth.2727>.
- Liao, H.Y., Frank, J., 2010. Definition and estimation of resolution in single-particle reconstructions. *Structure* 18, 768–775. <https://doi.org/10.1016/j.str.2010.05.008>.
- Liebschner, D., Afonine, P.V., Baker, M.L., Bunkóczi, G., Chen, V.B., Croll, T.I., Hintze, B. J., Hung, L.-W., Jain, S., McCoy, A.J., Moriarty, N.W., Oeffner, R.D., Poon, B.K., Prisant, M.G., Read, R.J., Richardson, J.S., Richardson, D.C., Sammito, M.D., Sobolev, O.V., Stockwell, D.H., Terwilliger, T.C., Urzhumtsev, A., Videau, L.L., Williams, C.J., Adams, P.D., 2019. Macromolecular structure determination using X-rays, neutrons and electrons: recent developments in Phenix. *Acta Crystallogr. D75*, 861–877. <https://doi.org/10.1107/S2059798319011471>.
- Lunin, V.Y., Urzhumtsev, A.G., 1984. Improvement of protein phases by coarse model modification. *Acta Crystallogr. A40*, 269–277. <https://doi.org/10.1107/S0108767384000544>.
- Lunin, V.Y., Lunina, N.L., Petrova, T.E., Baumstark, M.W., Urzhumtsev, A., 2019. Mask-based approach to phasing of single-particle diffraction data. II. Likelihood based selection criteria. *Acta Crystallogr. D75*, 79–89. <https://doi.org/10.1107/S2059798318016959>.
- Minichino, A., Habash, J., Raftery, J., Helliwell, J.R., 2003. The properties of $(2F_0 - F_0)$ and $(F_0 - F_0)$ electron-density maps at medium-to-high resolutions. *Acta Crystallogr. D59*, 843–849. <https://doi.org/10.1107/S0907444903004219>.
- Mooij, W.T.M., Hartshorn, M.J., Tickle, I.J., Sharff, A.J., Verdonk, M.L., Jhoti, H., 2006. Automated protein-ligand crystallography for structure-based drug design. *ChemMedChem* 1, 827–838. <https://doi.org/10.1002/cmdc.200600074>.
- Penczek, P.A., 2010. Resolution measures in molecular electron microscopy. *Methods Enzymol.* 482, 73–100. [https://doi.org/10.1016/S0076-6879\(10\)82003-8](https://doi.org/10.1016/S0076-6879(10)82003-8).

- Peng, L.-M., 1999. Electron atomic scattering factors and scattering potentials of crystals. *Micron* 30, 625–648. [https://doi.org/10.1016/S0968-4328\(99\)00033-5](https://doi.org/10.1016/S0968-4328(99)00033-5).
- Petersen, E.F., Goddard, T.D., Huang, C.C., Couch, G.S., Greenblatt, D.M., Meng, E.C., Ferrin, T.E., 2004. UCSF Chimera—a visualization system for exploratory research and analysis. *J. Comput. Chem.* 25, 1605–1612. <https://doi.org/10.1002/jcc.20084>.
- Pintilie, G., Chiu, W., 2012. Comparison of Segger and other methods for segmentation and rigid-body docking of molecular components in cryo-EM density maps. *Biopolymers* 97, 742–760. <https://doi.org/10.1002/bip.22074>.
- Pintilie, G., Zhang, K., Su, Z., Li, S., Schmid, M.F., Chiu, W., 2020. Measurement of atom resolvability in cryo-EM maps with Q-scores. *Nat. Methods* 17, 328–334. <https://doi.org/10.1038/s41592-020-0731-1>.
- Ramírez-Aportela, E., Mota, J., Conesa, P., Carazo, J.M., Sorzano, C.O.S., 2019. DeepRes: a new deep-learning- and aspect-based local resolution method for electron-microscopy maps. *Int. J. Cryst. 6*, 1054–1063. <https://doi.org/10.1107/S2052252519011692>.
- Read, R.J., 1986. Improved Fourier coefficients for maps using phases from partial structures with errors. *Acta Crystallogr. A* 42, 140–149. <https://doi.org/10.1107/S0108767386099622>.
- Rosenthal, P.B., Henderson, R., 2003. Optimal determination of particle orientation, absolute hand, and contrast loss in single-particle electron cryomicroscopy. *J. Mol. Biol.* 333, 721–745. <https://doi.org/10.1016/j.jmb.2003.07.013>.
- Rupp, B., 2009. *Biomolecular Crystallography. Principles, Practice, and Applications to Structural Biology*. Garland Science, Taylor & Francis Group, New York (USA).
- Saxton, W.O., Baumeister, W., 1982. The correlation averaging of a regularly arranged bacterial cell envelope protein. *J. Microsc.* 127, 127–138. <https://doi.org/10.1111/j.1365-2818.1982.tb00405.x>.
- Schrödinger, L., DeLano, W., 2020. Pymol. <http://www.pymol.org/pymol>.
- Simonetti, A., Marzi, S., Fabbretti, A., Myasnikov, A.G., Hazemann, I., Jenner, L., Urzhumtsev, A., Gualerzi, C.O., Klaholz, B.P., 2013. Crystal structure of the protein core of translation initiation factor IF2 in apo, GTP and GDP forms. *Acta Crystallogr. D* 69, 925–933. <https://doi.org/10.1107/S0907444913006422>.
- Terwilliger, T.C., Sobolev, O.V., Afonine, P.V., Adams, P.D., 2018. Automated map sharpening by maximization of detail and connectivity. *Acta Crystallogr. D* 74, 545–559. <https://doi.org/10.1107/S2059798318004655>.
- Urzhumtsev, A.G., Lunin, V.Y., 2019. Introduction to crystallographic refinement of macromolecular atomic models. *Crystallogr. Rev.* 25, 164–262. <https://doi.org/10.1080/0889311X.2019.1631817>.
- Urzhumtsev, A.G., Lunin, V.Y., 2022a. Analytic modeling of inhomogeneous-resolution maps in cryo-electron microscopy and crystallography. *IUCr Journal* 9, 728–734. <https://doi.org/10.1107/S2052252522008260>.
- Urzhumtsev, A.G., Lunin, V.Y., 2022b. Toward real real-space refinement of atomic models. *Int. J. Molec. Sciences* 23, 12101. <https://doi.org/10.3390/ijms232012101>.
- Urzhumtsev, A.G., Urzhumtseva, L.M., Lunin, V.Y., 2022. Direct calculation of cryo-EM and crystallographic model maps for real-space refinement. *Acta Crystallogr. D* 78, 1451–1468. <https://doi.org/10.1107/S2059798322010907>.
- Urzhumtseva, L., Klaholz, B.P., Urzhumtsev, A.G., 2013. On effective and optical resolution of diffraction data sets. *Acta Crystallogr. D* 69, 1921–1934. <https://doi.org/10.1107/S0907444913016673>.
- Urzhumtseva, L.M., Lunin, V.Y., Urzhumtsev, A.G., 2023. Algorithms and programs for the shell decomposition of oscillating functions in space. *J. Appl. Crystallogr.* 56, 302–311. <https://doi.org/10.1107/S160057672201144X>.
- Vaguine, A.A., Richelle, J., Wodak, S., 1999. SFCHECK: a unified set of procedures for evaluating the quality of macromolecular structure-factor data and their agreement with the atomic model. *Acta Crystallogr. D* 55, 191–205. <https://doi.org/10.1107/S0907444998006684>.
- van Heel, M., Schatz, M., 2017. Reassessing the Revolution's Resolutions. *BioRxiv*. <https://doi.org/10.1101/224402>.
- van Heel, M., Keegstra, W., Schutter, W., van Bruggen, E.F.J., 1982. The structure and function of invertebrate respiratory proteins. EMBO workshop. In: Wood, E.J. (Ed.), *Life Chemistry Reports Suppl. 1. The Structure and Function of Invertebrate Respiratory Proteins*. EMBO workshop, Leeds, pp. 69–73.
- Vilas, J.L., Gómez-Blanco, J., Conesa, P., Melero, R., de la Rosa-Trevín, J.M., Otón, J., Cuenca, J., Marabini, R., Carazo, J.M., Vargas, J., Sorzano, C.O.S., 2018. MonoRes: automatic and accurate estimation of local resolution for electron microscopy maps. *Structure* 26, 337–344. <https://doi.org/10.1016/j.str.2017.12.018>.
- Wang, J., Natchiar, S.K., Moore, P., Klaholz, B., 2021. Identification of Mg 2+ ions next to nucleotides in cryo-EM maps using electrostatic potential maps. *Acta Crystallogr. D* 77, 534–539. <https://doi.org/10.1107/S2059798321001893>.
- Zivanov, J., Nakane, T., Forsberg, B.O., Kimanius, D., Hagen, W.J., Lindahl, E., Scheres, S.H., 2018. New tools for automated high-resolution cryo-EM structure determination in RELION-3. *Elife* 7, e42166. <https://doi.org/10.7554/eLife.42166>.